MOLECULAR IMAGING AND BIOLOGY

Mol Imaging Biol (2019) 21:825–834
DOI: 10.1007/s11307-018-01303-4

Published Online: 3 January 2019

RESEARCH ARTICLE

Imaging of the Mouse Lymphatic Sinus during Early Stage Lymph Node Metastasis Using Intranodal Lymphangiography with X-ray Micro-computed Tomography

Ryo Iwamura,[1,2] Maya Sakamoto,[3] Shiro Mori,[1,2,4] Tetsuya Kodama[1,2]

[1]*Laboratory of Biomedical Engineering for Cancer, Graduate School of Biomedical Engineering, Tohoku University, 4-1 Seiryo, Aoba, Sendai, Miyagi, 980-8575, Japan*
[2]*Biomedical Engineering Cancer Research Center, Graduate School of Biomedical Engineering, Tohoku University, 4-1 Seiryo, Aoba, Sendai, Miyagi, 980-8575, Japan*
[3]*Department of Oral Diagnosis, Tohoku University Hospital, 1-1 Seiryo, Aoba, Sendai, Miyagi, 980-8574, Japan*
[4]*Department of Oral and Maxillofacial Surgery, Tohoku University Hospital, 1-1 Seiryo, Aoba, Sendai, Miyagi, 980-8575, Japan*

Abstract

Purpose: Lymph node (LN) metastasis is detected prior to distant metastasis in many types of cancer. Detecting early stage LN metastasis can improve treatment outcomes. However, there are few clinical imaging modalities capable of diagnosing metastatic LNs of clinical N0 status (i.e., before their volume increases) with high precision. Here, we report a new method for diagnosing metastatic LNs of clinical N0 status in a mouse model of LN metastasis.

Procedures: The method involved using intranodal lymphangiography with x-ray micro-computed tomography (micro-CT). Contrast agent was injected into an upstream LN to deliver it to a downstream LN, which was then removed and analyzed by micro-CT.

Results: We found that using an intranodal injection rate of 10–60 μl/min filled the lymphatic sinus of the downstream LN with contrast agent, although the accumulation of contrast agent in the upstream LN increased with a faster injection rate. Furthermore, breast cancer cells growing in the lymphatic sinus of the downstream LN (which was of clinical N0 status) impeded the flow of contrast agent from the upstream LN, resulting in areas deficient of contrast agent in the metastatic downstream LN. The formation of defect areas in the downstream LN manifested as a difference in position between the centroid of the entire LN area and the centroid of the region that filled with contrast agent.

Conclusion: The present study indicates that intranodal lymphangiography with micro-CT has the potential to be used as a new method for diagnosing metastatic LNs of clinical N0 status.

Key words: Intranodal lymphangiography, Lymph node, Metastasis, Clinical N0, CT, Micro-CT, Sentinel lymph node

Introduction

Lymph node (LN) metastasis is detected prior to distant metastasis in many cancers. Since there is a strong association between LNs and distant metastasis [1], the

Electronic supplementary material The online version of this article (https://doi.org/10.1007/s11307-018-01303-4) contains supplementary material, which is available to authorized users.

Correspondence to: Tetsuya Kodama; *e-mail:* kodama@tohoku.ac.jp

early diagnosis of LN metastasis can improve treatment outcomes [2]. Nodal staging is achieved using a combination of multiple imaging modalities such as computed tomography (CT), magnetic resonance imaging (MRI), ultrasound (US), and positron emission tomography. However, precise examination of LNs with a maximal short-axis diameter less than 10 mm is difficult to achieve with these imaging modalities. Although LN biopsy is an important method for determining whether LN dissections are necessary, the false negative rate of sentinel node biopsy for breast cancer has been reported to be 7.3–9.7 % in large-scale clinical trials and meta-analyses [3–6].

Growth and progression of a primary tumor induce structural changes in tumor-draining LNs and lymphatic vessels, resulting in alterations in lymph flow dynamics [7]. Tumor cells that reach the marginal sinus of a tumor-draining LN invade into the vessels beneath the LN capsule, and as a result, the tumor-draining LN functions as a source of systemic metastasis (i.e., LN-mediated hematogenous metastasis theory) [8, 9]. Recent studies have provided additional evidence in support of this theory of metastasis [10, 11]. Tumor cells in the marginal sinus continue to grow and develop, and subsequently, the size of the lymphatic sinus decreases [12] and intranodal pressure increases [13]. Since little or no angiogenesis is observed in metastatic LNs [14, 15], the subsequent response to intravenous chemotherapy becomes low. Thus, new techniques for diagnosing and treating early stage LN metastasis (i.e., LNs that contain metastasis but are of clinical N0 status) are needed to prevent systemic metastasis [2].

Lymphangiography is a method of visualizing the lymphatic system that relies on the injection of radiopaque material into a lymphatic vessel [16, 17]. In breast cancer, 3D-CT lymphangiography can provide a detailed description of the lymphatic vessels between the primary tumor and sentinel LN and identify the sentinel LN, and this technique is superior to staining with dyes or radioisotope incorporation [18]. In addition, 3D-CT lymphangiography has been used to detect defects in the staining of sentinel LNs and obstruction, stagnation, dilation, and detour of lymphatic vessels due to tumor occupation [19]. Intranodal lymphangiography has also provided new clinical insights into lymphatic pathology [20].

The aim of the present study was to develop a new method of diagnosing metastatic LNs of clinical N0 status in a mouse model of LN metastasis [12, 21] using x-ray micro-computed tomography (micro-CT) with intranodal lymphangiography. In general, there are two types of LN in the axillary area in a mouse: the proper axillary LN (PALN) and accessory axillary LN (AALN). The subiliac LN (SiLN) and AALN are upstream of the PALN in the lymphatic system [8]. First, we identified the optimal rate of contrast agent injection into the SiLN for delivery of contrast agent to the PALN. Next, tumor cells were injected into the SiLN to induce metastasis in the PALN, such that the PALN was of clinical N0 status (i.e., no major increase in volume). Then, contrast agent was injected into the AALN to deliver it to the PALN. The effectiveness of intranodal lymphangiography in the detection of PALN metastasis was evaluated by visualizing the harvested PALN using micro-CT.

Materials and Methods

All *in vivo* studies were approved by the Institutional Animal Care and Use Committee of Tohoku University (permit numbers: 2016BeLMO-015, 2017BeLMO-003, 2016BeA-0018, and 2017BeA-009). All experiments were performed in accordance with relevant guidelines and regulations.

Mice

The MXH10/Mo/lpr mouse strain [22] is a substrain of the recombinant inbred strain of the MXH/lpr mouse [23]. MXH10/Mo/lpr mice (16–18 weeks of age) were bred under specific pathogen-free conditions in the Animal Research Institute, Tohoku University. MXH/lpr mice were generated using two different parental inbred strains as progenitors, MRL/lpr (major histocompatibility complex; H-2^k) and C3H/lpr (H-2^k), followed by an F1 intercross and more than 20 generations of strict brother-sister mating. MXH10/Mo/lpr mice are unique; their most peripheral LNs grow to about 10 mm in size at 2.5 to 3 months of age, and the mice do not develop severe autoimmune diseases.

Barium Contrast Agent for Micro-CT

First, 50.0 g of barium sulfate (Enemaster; Fushimi Pharmaceutical Co. Ltd., Kagawa, Japan) was dissolved in 83.7 ml of normal saline at 50 °C. The resulting solution was mixed with 3.1 g of gelatin (Morinaga & Co. Ltd., Tokyo, Japan) and 5.7 ml of red acrylics (Liquitex; cadmium red medium, soft type; BonnyColArt Co. Ltd., Tokyo, Japan) to make the barium contrast agent [24]. The size of the contrast agent was 1.0 ± 0.3 μm.

Optimization of the Rate of Contrast Agent Injection into the AALN

Each mouse was anesthetized with 2 % isoflurane (Abbott Japan Co. Ltd., Tokyo, Japan) in O_2 and placed on a pad heated to 37 °C. To deliver contrast agent to the PALN, a syringe pump (Legato100; KD Scientific, Holliston, MA, USA) connected to a 1-ml syringe with a 27G winged intravenous needle (Terumo, Tokyo, Japan) was used to inject 120 μl of contrast agent (pre-warmed to 50 °C) into the AALN of the mouse at rates of 10.0 μl/min, 30.0 μl/min, or 60.0 μl/min. After injection of the contrast agent, the

PALN and AALN were dissected and fixed in 10 % neutral buffered formalin solution at 4 °C for 4 days.

Intranodal Lymphangiography Using Micro-CT

The lymphatic sinuses in the PALN and AALN were visualized using a micro-CT scanner that was developed specifically to image small experimental laboratory animals (LaTheta LCT-200; Hitachi-Aloka Medicals, Tokyo, Japan). The spatial resolution was 8–20 μm, and the image data acquired consisted of 1024 × 1024 × 1008 pixels. The acquired slice data were rendered as 3D images using a 3D analysis suite (ConeCTexpress; WhiteRabbit Corp., Tokyo, Japan) and analyzed using 3D visualization and analysis software (Amira; Maxnet Co. Ltd., Tokyo, Japan).

Cell Culture

C3H/He mouse mammary carcinoma cells (FM3A-Luc), stably expressing the Luc gene [22], were used. Cell were incubated (37 °C, 5 % CO_2/95 % air) until 80 % confluence was achieved. Lack of *Mycoplasma* contamination was confirmed on the inoculation day (MycoAlert *Mycoplasma* Detection Kit; Lonza Group, Basel, Switzerland). Cells expressed vascular endothelial growth factor (VEGF)-A and VEGF-B but not VEGF-C [13].

Induction of Metastasis in the PALN (N0 Status) by Injection of Tumor Cells into the SiLN

The mice were divided into the following groups: day 14 ($n = 4$), day 21 ($n = 3$), and day 28 ($n = 4$). FM3A-Luc cells (passaged three times) were suspended in 10-μl phosphate-buffered saline plus 20 μl of 400 mg/ml Matrigel (Collaborative Biomedical Products, Bedford, MA, USA) to a final cell concentration of 3.3×10^5 cells/ml. Each mouse was anesthetized with 2 % isoflurane in O_2 and placed on a heated pad (37 °C). A 60-μl volume of the prepared cell solution was injected into the SiLN *via* a 27G winged intravenous needle (Terumo); the injection was carried out under high-frequency US guidance (VEVO770, VisualSonics, Toronto, Canada), using a 25-MHz transducer (RMV-710B; axial resolution, 70 μm; focal length, 15 mm; VisualSonics). The day of tumor cell inoculation was defined as day 0 [25]. PALN tumor growth was assessed using an *in vivo* bioluminescence imaging system (*in vivo* imaging system (IVIS); PerkinElmer, Waltham, MA, USA). The luciferase activities of FM3A-Luc cells were measured at days 0 and 14 for the day 14 group, days 0 and 21 for the day 21 group, and days 0 and 28 for the day 28 group. At each time point, luciferase activity was measured 10 min after intraperitoneal injection of luciferin (150 mg/kg; Promega, Madison, WI, USA) under anesthesia (2 % isoflurane in O_2).

Measurement of the Volume of the Metastatic PALN at N0 Status

Each mouse was anesthetized with 2 % isoflurane in O_2 and positioned on a heated pad (37 °C). The volume of the PALN was measured using a high-frequency US system (VEVO770; VisualSonics) equipped with a 25-MHz transducer (RMV-710B; VisualSonics). For experiments utilizing FM3A-Luc cells, PALN volume was measured at days 0 and 14 for the day 14 group, days 0 and 21 for the day 21 group, and days 0 and 28 for the day 28 group.

Imaging of the Metastatic PALN (at N0 Status) and AALN Using Intranodal Lymphangiography

Images of the PALN and AALN were obtained on the appropriate day according to the group name (e.g., at day 3 for the day 3 group, day 6 for the day 6 group, and so on). Each mouse was anesthetized with 2 % isoflurane in O_2 and placed on a heated pad (37 °C). A 1-ml syringe with a 27G winged intravenous needle (Terumo), connected to a syringe pump (Legato100; KD Scientific) was used to inject 120 μl of contrast agent (pre-warmed to 50 °C) into the AALN at a rate of 10 μl/min, so that the contrast agent was delivered to the PALN. Then, the PALN and AALN were dissected and fixed in 10 % neutral buffered formalin solution at 4 °C for 4 days.

Analysis of Intranodal Structures Using a Micro-CT Scanner

The intranodal structures of the PALN and AALN were visualized using a micro-CT scanner (LaTheta LCT-200; Hitachi-Aloka Medicals). The spatial resolution was 8–20 μm, and the image data acquired consisted of 1024 × 1024 × 1008 pixels. The acquired slice data were rendered as 3D images using a 3D analysis suite (ConeCTexpress; WhiteRabbit Corp.) and analyzed using 3D visualization and analysis software (Amira; Maxnet Co. Ltd). Three-dimensional images of the LN and of the intranodal region containing contrast medium were extracted from the CT data. LN imaging was carried out with the LN placed in a plastic tube that was positioned on the platform. Each volume was calculated from the obtained data, and the ratio of the contrast region volume to the total LN volume was calculated. The difference in the distance between the centroid ("center of gravity") of the entire LN and the centroid of the region containing contrast medium was obtained from the analysis data. LN extraction was achieved by selecting outside the air region by threshold value, then manually removing the platform and the plastic tube part and selecting inside the LN. For extraction of the region containing contrast medium, part of the region within the LN (including soft tissue) into which contrast medium had flowed was selected, and the threshold value was set as half

the average CT value in that region. Data after reconstruction was saved as 16-bit DICOM data.

Histological Analysis

After being imaged by intranodal lymphangiography, the PALN and AALN tissues were dehydrated, embedded in paraffin, serially sectioned (3–4 μm) and either stained with hematoxylin and eosin (HE) or immunostained for LYVE-1-positive and CD31-positive cells (Discovery XT Automated Staining Processor; Ventana Medical Systems, Tucson, AZ, USA) [12, 13, 25].

Statistical Analysis

All data are expressed as the mean ± standard error of the mean (SEM). Comparisons between groups were made using one- or two-way repeated measures analysis of variance (ANOVA), the Kruskal-Wallis test, Tukey-Kramer test, or Pearson correlation test, as appropriate. $P < 0.05$ was regarded as a statistically significant difference.

Results

Optimization of the Rate of Contrast Agent Injection into the Upstream LN for Effective Delivery to the Downstream LN

To determine the optimal injection rate for delivery of contrast agent from the AALN to the PALN, contrast agent was injected into the AALN at various rates (10, 30, and 60 μl/min), and micro-CT imaging was used to evaluate the AALN and PALN after their removal from the mouse (Fig. 1a). Imaging of the AALN revealed that the area filled with contrast agent increased with increasing injection rate.

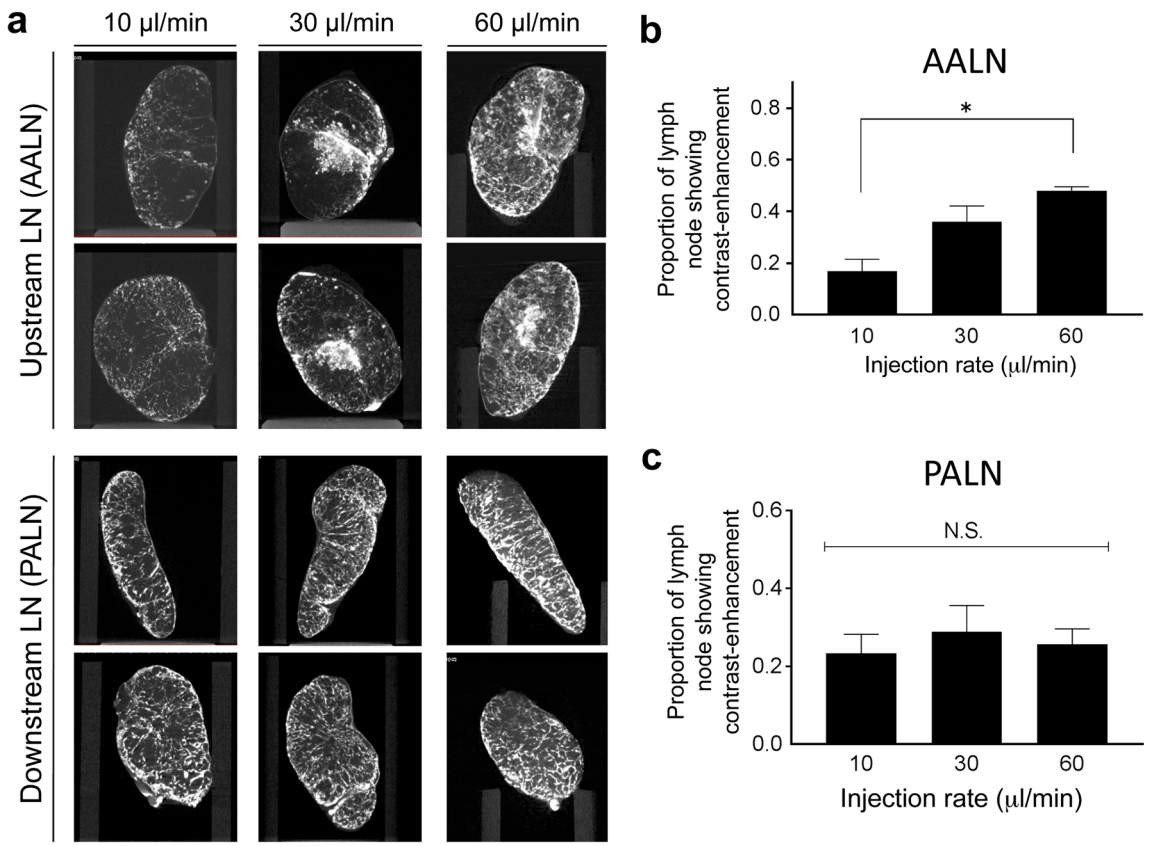

Fig. 1 Visualization of the AALN and PALN by micro-CT. a AALN = The area of the AALN filled with contrast agent increased with increasing injection rate. Notable accumulation of contrast agent in the center of the AALN was observed for injection rates of 30 μl/min (**c**, **d**) and 60 μl/min (**e**, **f**). PALN = The contrast agent had entered the marginal, trabecular and medullary sinuses. There were no obvious differences between the images acquired for different injection rates. **b** Proportion of the AALN showing contrast-enhancement for each injection rate. The proportion of the AALN showing contrast-enhancement increased with increasing injection rate; 10 μl/min ($n = 4$), 30 μl/min ($n = 4$), and 60 μl/min ($n = 4$). Data are shown as the mean ± SEM. *$P < 0.05$, 10 μl/min vs. 60 μl/min (one-way ANOVA and Tukey-Kramer test). **c** Proportion of the PALN showing contrast-enhancement for each injection rate. There were no significant differences between the various injection rates; 10 μl/min ($n = 4$), 30 μl/min ($n = 4$), 60 μl/min ($n = 4$). Data are shown as the mean ± SEM.

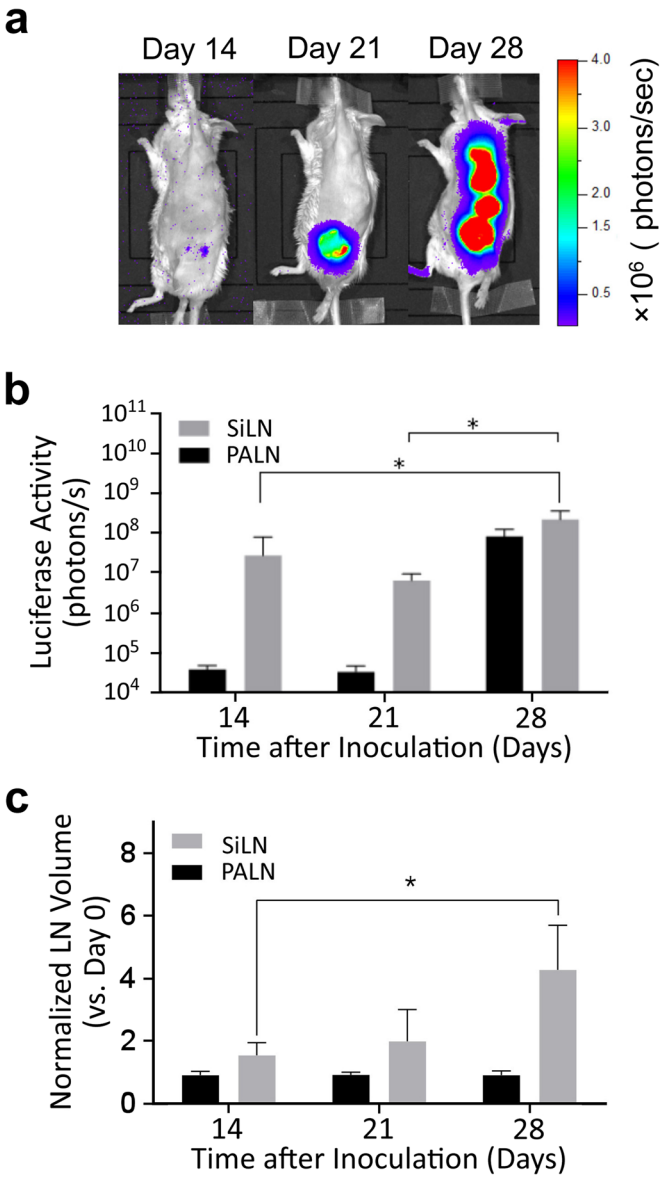

Fig. 2 Induction of metastasis in the PALN. Tumor cells were injected into the SiLN to induce metastasis to the PALN *via* lymphatic vessels. **a** *In vivo* bioluminescence imaging. Luciferase activity in the PALN was measured at days 14, 21, and 28. Metastasis was considered successfully induced when the PALN luciferase activity exceeded the background level in control experiments: this was day 28. **b** Luciferase activity. Luciferase activity increased with time after the inoculation. Day 14 ($n = 4$), day 21 ($n = 3$), and day 28 ($n = 4$). There were significant differences in luciferase activity among groups for the SiLN but not PALN. *$P < 0.01$, day 14 vs. day 28; *$P < 0.01$, day 21 vs. day 28; one-way ANOVA and Tukey-Kramer test. Data are shown as the mean ± SEM. **c** Changes in the volumes of the SiLN and PALN after tumor inoculation into the SiLN. There was a significant increase in the volume of the SiLN at day 28 (*$P < 0.05$, day 14 vs. day 28; one-way ANOVA and Tukey-Kramer test). The PALN after inoculation would be considered a LN with clinical N0 status. Day 14 ($n = 4$), day 21 ($n = 3$), and day 28 ($n = 4$). Data are shown as the mean ± SEM.

In particular, notable accumulation of contrast agent in the center of the AALN was observed at injection rates of 30 and 60 µl/min. Figure 1b shows the mean data for the proportion of the AALN showing contrast-enhancement for each injection rate: the proportion of the AALN showing contrast-enhancement increased with increasing injection rate ($P < 0.05$, 10 µl/min vs. 60 µl/min; one-way ANOVA and Tukey-Kramer test). Imaging of the PALN (Fig. 1a) showed that the contrast agent had reached the marginal, trabecular, and medullary sinuses, but there were no notable differences between images for the different injection rates. The mean proportion of the PALN showing contrast-enhancement did not differ significantly between injection rates (Fig. 1c). Based on these results, subsequent experiments utilized an injection rate of 10 µl/min for the delivery of contrast agent from the AALN to the PALN.

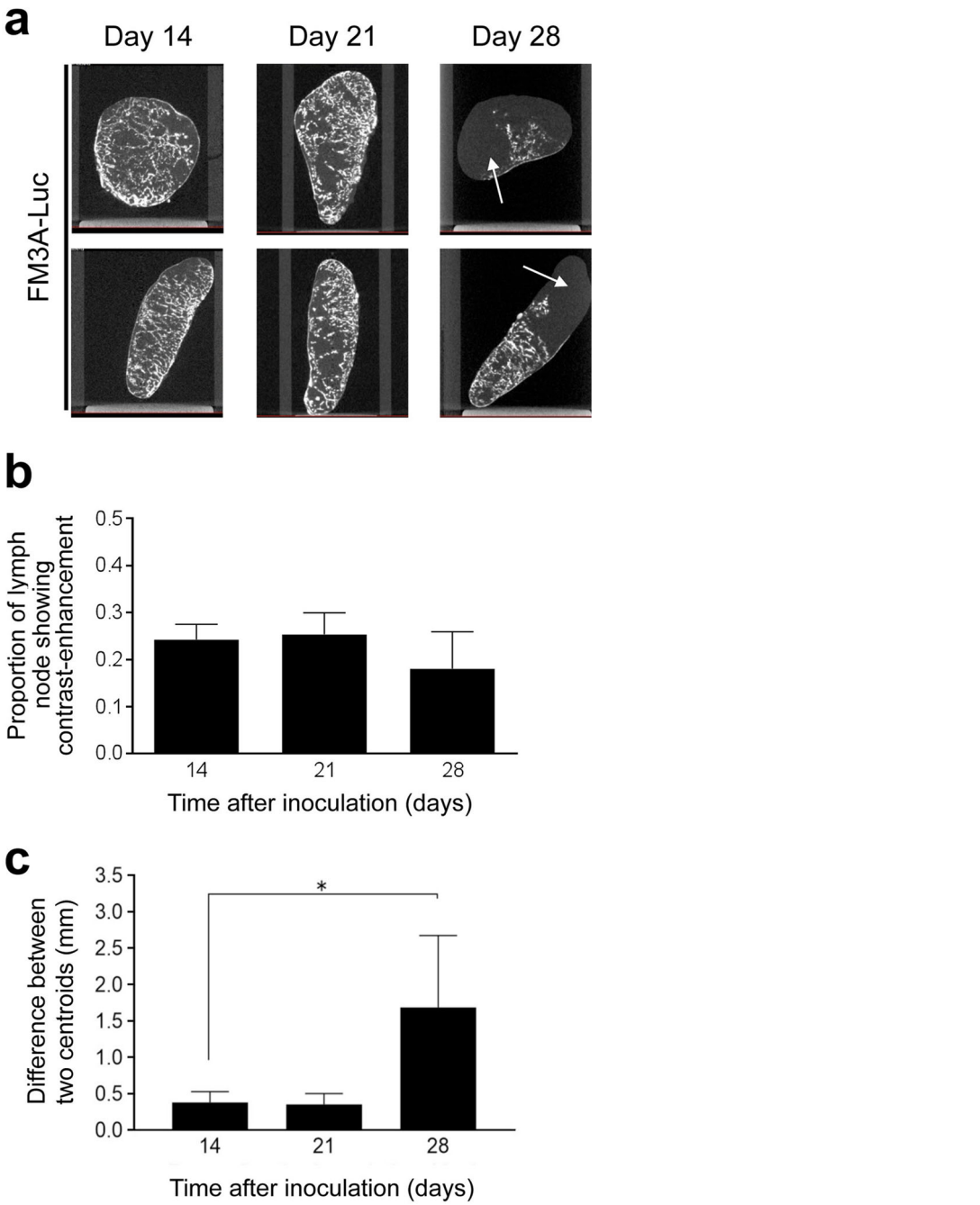

Fig. 3 PALN metastasis imaged by intranodal lymphangiography. **a** micro-CT images. Contrast agent was observed in the marginal, trabecular, and medullary sinuses at day 14 (Aa, Ab) and day 21 (Ac, Ad). Images are rotated around the axis. Defect areas (arrows) were observed at day 28 (Ae, Af). **b** Analysis of contrast-enhanced regions. The proportion of the PALN showing contrast-enhancement did not change significantly over time. Day 14 ($n = 4$), day 21 ($n = 3$), and day 28 ($n = 4$). Data are shown as the mean ± SEM. **c** Difference in position between the centroid of the entire PALN area and the centroid of the region filled with contrast agent. There was a significant change at day 28 ($^*P < 0.05$, day 14 vs. day 28; one-way ANOVA and Tukey-Kramer test). Day 14 ($n = 4$), day 21 ($n = 3$), and day 28 ($n = 4$). Data are shown as the mean ± SEM.

Luciferase Activity in the SiLN and PALN after Tumor Inoculation into the SiLN

Next, we evaluated whether intranodal lymphangiography could be used to evaluate LNs of clinical N0 status (Fig. 2). Tumor cells were injected into the SiLN to induce metastasis to the PALN. *In vivo* bioluminescence images and luciferase activities are shown in Fig. 2a. Metastasis was detected in the PALN at day 28 after inoculation. The luciferase activity increased with time in both the PALN

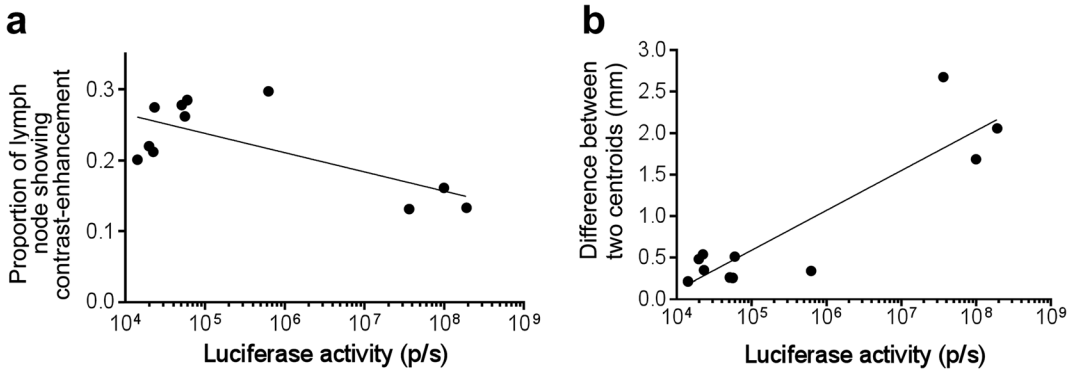

Fig. 4 Correlations of the proportion of the PALN showing contrast-enhancement and the positional difference between the two centroids with luciferase activity in the PALN. **a** Correlation of the proportion of the PALN showing contrast-enhancement with luciferase activity. There was a significant correlation between the two parameters (Pearson correlation test: $R^2 = 0.50$). **b** Correlation of the difference between the two centroids with luciferase activity. There was a significant correlation between the two parameters (Pearson correlation test: $R^2 = 0.51$).

and SiLN (Fig. 2b), and significant changes were observed for the SiLN ($P < 0.01$, day 14 vs. day 28; $P < 0.01$, day 21 vs. day 28; two-way ANOVA and Tukey-Kramer test).

Changes in the Volumes of the SiLN and PALN after Tumor Inoculation into the SiLN

Next, we investigated whether volume changes occurred in the SiLN and PALN after inoculation of tumor cells (Fig. 2c). The SiLN volume was significantly increased at day 28 ($P < 0.05$, day 14 vs. day 28; one-way ANOVA and Tukey-Kramer test). There were no significant changes in PALN volume. Therefore, the PALN after inoculation would be considered a LN with clinical N0 status.

PALN Metastasis Imaged by Intranodal Lymphangiography

Subsequently, we imaged the metastatic PALN (of clinical N0 status) using intranodal lymphangiography; for these experiments, the contrast agent was injected into the AALN at a rate of 10 µl/min. Contrast agent was observed in the marginal, trabecular, and medullary sinuses at days 14 (Fig. 3a, Supplemental Movie 1) and 21 (Fig. 3a, Supplemental Movie 2), and defect areas (arrows) were observed at day 28 (Fig. 3a, Supplemental Movie 3). The proportion of the PALN showing contrast-enhancement showed little or no change between days 14, 21, and 28 (Fig. 3b).

The distribution of the contrast agent in the PALN was evaluated by measuring the positional difference between the centroid of the entire PALN area and the centroid of the region that filled with contrast agent (Fig. 3c). A significant change was observed at day 28 ($P < 0.05$, day 14 vs. day 28; one-way ANOVA and Tukey-Kramer test). Thus, the presence of defect areas in the PALN on day 28 manifested as an increase in the difference between the positions of the two centroids.

Figure 4a shows that there was a significant correlation between the proportion of the PALN showing contrast-enhancement and the luciferase activity in the PALN (Pearson correlation test: $R^2 = 0.50$). The positional difference between the two centroids and the luciferase activity in the PALN also showed a significant correlation (Pearson correlation test: $R^2 = 0.51$, Fig. 4b).

Pathological changes in the PALN were also examined (Fig. 5a, b). Areas of tumor invasion (Fig. 5c–e, which are enlarged images of region (ii) in Fig. 5b) and areas without tumor invasion (Fig. 5f–h, which are enlarged images of region (iii) in Fig. 5b) were detected. Contrast agent was not detected in the region of the lymphatic sinus where tumor cells had invaded (Fig. 5c) but was evident in the region of the lymphatic sinus without tumor cells (Fig. 5f). These results suggest that the size of the contrast-enhanced area would decrease following the invasion of tumor cells into the lymphatic sinus. Tumor angiogenesis and lymphangiogenesis were not detected near the lymphatic sinus (Fig. 5d, e.

Discussion

The development of new imaging modalities to detect metastatic LNs that are still of clinical N0 status would likely lead to improvements in the prognosis and quality of life of people with cancer. Conventional mouse models of cancer use experimental mice with LNs that are 1–2 mm in diameter; hence, these models may not be representative of human LN metastasis [26]. The present study was designed to develop a new imaging method for the diagnosis of metastasis in LNs of clinical N0 status, using intranodal lymphangiography in a model of LN metastasis developed with MXH10/Mo/lpr mice.

First, the intranodal injection rate was optimized to deliver contrast agent from the upstream LN (AALN) to the downstream LN (PALN) and ensure that the PALN would be filled with contrast agent. Increasing the intranodal injection rate from 10 to 60 µl/min resulted in greater accumulation of contrast agent in the AALN (Fig. 1b) but did not cause a significant increase in the amount of contrast agent delivered to the PALN (Fig. 1c). Therefore, the optimal rate for intranodal injection into the upstream LN was considered to be 10 µl/min. Fujii et al. [27] injected fluorescent dye into the SiLN (to deliver it to the PALN) of MXH10/Mo/lpr mice at various rates (10, 20, 40, 60, 80, 100 and 2400 µl/min [bolus injection]) and concluded from the distribution of dye in the PALN that the optimal

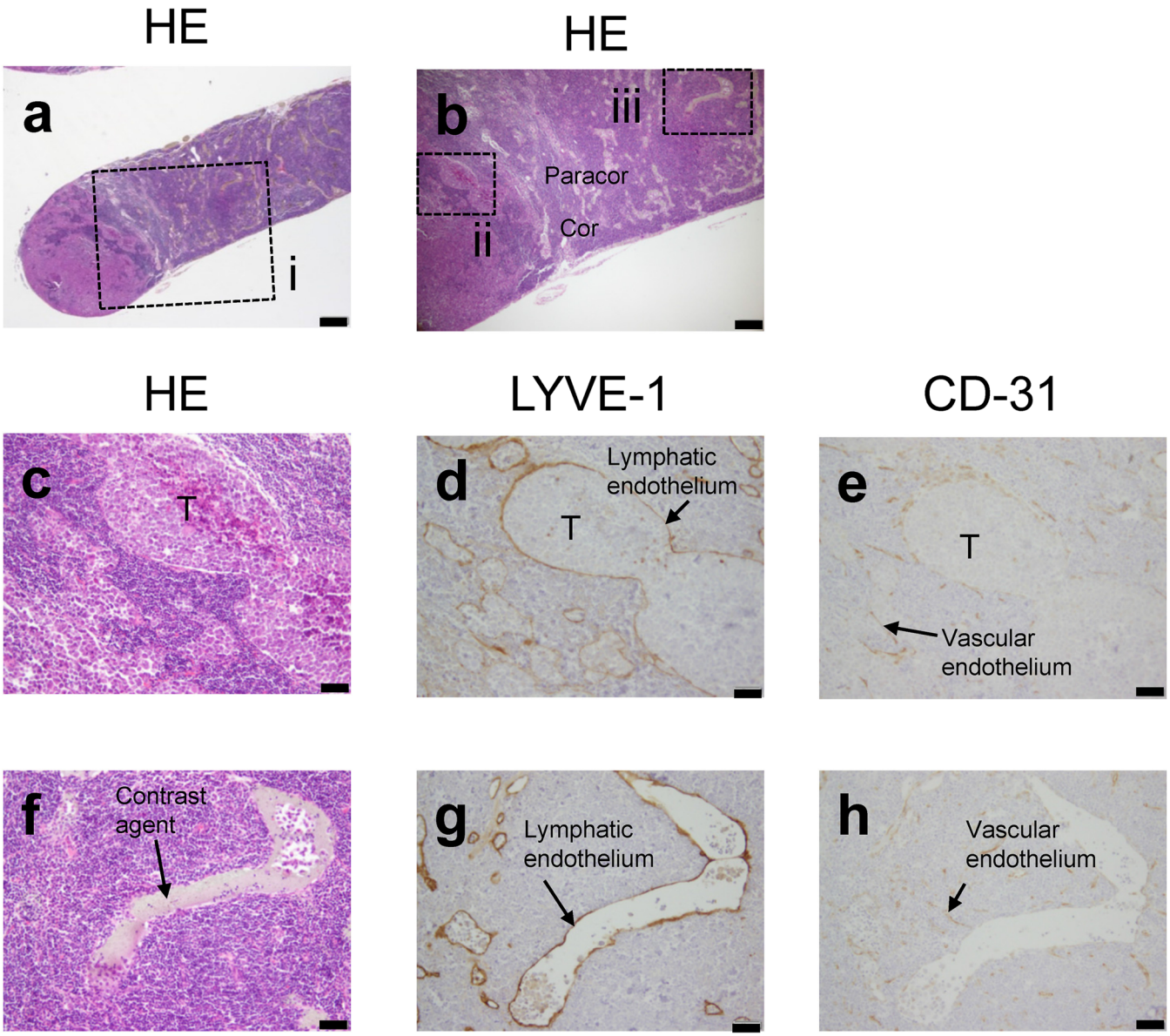

Fig. 5 Histological analysis of the metastatic PALN. Contrast agent was delivered from the AALN to the PALN at day 28. **a** HE staining showing tumor cell invasion into the PALN. Scale bar = 500 µm. **b** Enlarged image of region (i) in a (HE staining). Regions showing tumor invasion (ii) not showing tumor invasion (iii) were evident. Scale bar = 200 µm. **c**–**e** Serial sections showing enlarged images of region (ii) in **b** tumor cells had invaded the lymphatic sinus, and contrast agent was not detected in the area of tumor cell invasion. **c** HE staining. Tumor cells had invaded the lymphatic sinus. Scale bar = 50 µm. **d** Immunostaining of LYVE-1. Tumor cells had invaded the lymphatic sinus. Scale bar = 50 µm. **e** Immunostaining of CD31. Tumor cells had invaded the lymphatic sinus. Scale bar = 50 µm. **f**–**h** Serial sections showing enlarged images of region (iii) (**b**). **f** HE staining. Tumor cells were not present in the lymphatic sinus, whereas contrast agent was detected. Scale bar = 50 µm. **g** Immunostaining of LYVE-1. Tumor cells were not observed in the lymphatic sinus. Scale bar = 50 µm. **h** Immunostaining of CD31. Tumor cells were not detected in the lymphatic sinus. Scale bar = 50 µm.

injection rate was between 10 and 80 μl/min. These observations were consistent with calculations of impulse values in the PALN from the injection pressures, and it was found that fluid driven into the PALN at a high injection rate (e.g., bolus injection) tended to flow into the marginal sinus but not cortex or trabecular sinus, whereas fluid driven into the PALN at a low injection rate (e.g., 10 μl/min) was able to penetrate into the cortex and trabecular sinus.

Dynamic contrast-enhanced MR lymphangiography has been developed recently using a combination of intranodal lymphangiography, gadolinium-based contrast agents and dynamic contrast-enhanced MR, and this technique has been used to visualize the central lymphatic system including LNs [28]. However, in view of the findings of Fujii and colleagues [27], lymphangiography using manual injection of contrast agent into a LN (rather than a slow, controlled infusion) might result in visualization of LNs bathed with contrast agent that had leaked onto their surfaces rather than LNs filled with contrast agent.

In this study, we evaluated the effectiveness of intranodal lymphangiography with micro-CT in the detection of metastatic LNs of clinical N0 status in our mouse model of LN metastasis. At the initial stage of tumor cell arrival in the lymphatic sinus of the PALN, the lymphatic, trabecular, and medullary sinuses were all filled with contrast agent (Fig. 3a at days 14 and 21). The inflow of contrast agent into blood vessels was not observed anywhere within the LN. Defect areas into which contrast agent did not flow were detected at day 28 (Fig. 3a). Within the defect areas, the lymphatic sinus was filled with tumor cells that had invaded the cortex, and invasion and growth of tumor cells were observed in the lymphatic stroma (Fig. 5a). Furthermore, the position of the centroid for the area filled with contrast agent varied due to the invasion and growth of tumor cells (Fig. 3c).

In a clinical study using MRI with lymphotropic superparamagnetic nanoparticles, intravenously injected nanoparticles gained access to the interstitium and were drained through lymphatic vessels at 24 h after injection [29]. Nanoparticles were internalized by macrophages in normal LNs causing changes in magnetic properties detectable by MRI. In metastatic LNs, a limited decrease in signal intensity or discrete focal defects were detected because the intranodal structure was replaced by tumor cells [29, 30]. The defective area observed in this study has nothing to do with uptake by macrophages. Instead, the proportion of the lymphoid sinuses that contained contrast agent decreased due to the proliferation of tumor cells in the LN, generating a defective region.

Some studies have reported that tumor cells can induce lymphangiogenesis in the sentinel LNs [7, 31, 32]. In the present study, we did not obtain any clear evidence of angiogenesis or lymphangiogenesis in the PALN in experiments utilizing FM3A-Luc cells (Fig. 5). Our experimental model induces metastasis in the PALN by injecting tumor cells into the SiLN so that they are delivered to the PALN via lymphatic vessels, and this method of metastasis may not follow the process of lymphatic metastasis related to the VEGF-C/VEGF-D/VEGFR-3 signaling axis. Therefore, lymphangiogenesis may not be induced in this model.

Studies using MXH10/Mo/lpr mice, which develop systemic swelling of LNs up to 10 mm in diameter at 2.5–3 months of age, have revealed that there are many blood vessel branches that penetrate the LN capsule and connect vessels that lie interior and exterior to the capsule. We have confirmed that this anatomical feature is also seen in C57BL6, BALB/c, and SCID mice, which have LNs of sizes 1–2 mm and which have been used as models of LN metastasis [9]. This characteristic is also found in human LNs. It is thought that at the early stage of formation of LN metastasis in C57BL6, BALB/c, and SCID mice, extranodal infiltration occurs or the LNs are replaced with tumor cells [26]. In this regard, the LNs of MXH10/Mo/lpr mice seem to be closer to human LNs than those of other mice. The regions of the metastatic downstream LN that were deficient of contrast agent in this study likely reflect the situation that occurs in patients seen in clinical practice.

In conclusion, our results demonstrate that metastatic LNs of clinical N0 status can be detected by intranodal lymphangiography with micro-CT. Further research is needed to optimize the contrast agent and develop high-precision imaging modalities and improved image processing methods.

Acknowledgements. The authors would like to thank T. Sato for technical assistance and the Biomedical Research Core of Tohoku University Graduate School of Medicine for technical support.

Contributions. RI, SM, and TK designed the present study. RI, SM, and KT performed the experiments. RI, SM, and TK drafted the manuscript and prepared the figures. RI, MS, SM, and TK interpreted the data. All authors reviewed the manuscript.FundingThe study was supported by JSPS KAKENHI grant numbers 18H03544 (MS), 17K20077 (TK), and 17H00865 (TK).

Compliance with Ethical Standards

Conflict of Interest

The authors declare that they have no conflict of interest.

References

1. Dieterich LC, Detmar M (2016) Tumor lymphangiogenesis and new drug development. Adv Drug Deliv Rev 99:148–160
2. Kodama T, Matsuki D, Tada A, Takeda K, Mori S (2016) New concept for the prevention and treatment of metastatic lymph nodes using chemotherapy administered via the lymphatic network. Sci Rep 6:32506
3. Clarke M, Collins R, Darby S, Davies C, Elphinstone P, Evans V, Godwin J, Gray R, Hicks C, James S, MacKinnon E, McGale P, McHugh T, Peto R, Taylor C, Wang Y, Early Breast Cancer Trialists' Collaborative Group (EBCTCG) (2005) Effects of radiotherapy and of differences in the extent of surgery for early breast cancer on local recurrence and 15-year survival: an overview of the randomised trials. Lancet 366:2087–2106

4. Kim T, Giuliano AE, Lyman GH (2006) Lymphatic mapping and sentinel lymph node biopsy in early-stage breast carcinoma: a metaanalysis. Cancer 106:4–16
5. Krag DN, Anderson SJ, Julian TB, Brown AM, Harlow SP, Ashikaga T, Weaver DL, Miller BJ, Jalovec LM, Frazier TG, Noyes RD, Robidoux A, Scarth HM, Mammolito DM, McCready D, Mamounas EP, Costantino JP, Wolmark N, National Surgical Adjuvant Breast and Bowel Project (2007) Technical outcomes of sentinel-lymph-node resection and conventional axillary-lymph-node dissection in patients with clinically node-negative breast cancer: results from the NSABP B-32 randomised phase III trial. Lancet Oncol 8:881–888
6. Veronesi U, Paganelli G, Viale G, Luini A, Zurrida S, Galimberti V, Intra M, Veronesi P, Maisonneuve P, Gatti G, Mazzarol G, de Cicco C, Manfredi G, Fernández JR (2006) Sentinel-lymph-node biopsy as a staging procedure in breast cancer: update of a randomised controlled study. Lancet Oncol 7:983–990
7. Karaman S, Detmar M (2014) Mechanisms of lymphatic metastasis. J Clin Invest 124:922–928
8. Shao L, Takeda K, Kato S, Mori S, Kodama T (2015) Communication between lymphatic and venous systems in mice. J Immunol Methods 424:100–105
9. Takeda K, Mori S, Kodama T (2017) Study of fluid dynamics reveals direct communications between lymphatic vessels and venous blood vessels at lymph nodes of mice. J Immunol Methods 445:1–9
10. Brown M, Assen FP, Leithner A, Abe J, Schachner H, Asfour G, Bago-Horvath Z, Stein JV, Uhrin P, Sixt M, Kerjaschki D (2018) Lymph node blood vessels provide exit routes for metastatic tumor cell dissemination in mice. Science 359:1408–1411
11. Pereira ER, Kedrin D, Seano G, Gautier O, Meijer EFJ, Jones D, Chin SM, Kitahara S, Bouta EM, Chang J, Beech E, Jeong HS, Carroll MC, Taghian AG, Padera TP (2018) Lymph node metastases can invade local blood vessels, exit the node, and colonize distant organs in mice. Science 359:1403–1407
12. Li L, Mori S, Kodama M, Sakamoto M, Takahashi S, Kodama T (2013) Enhanced sonographic imaging to diagnose lymph node metastasis: importance of blood vessel volume and density. Cancer Res 73:2082–2092
13. Miura Y, Mikada M, Ouchi T, Horie S, Takeda K, Yamaki T, Sakamoto M, Mori S, Kodama T (2016) Early diagnosis of lymph node metastasis: importance of intranodal pressures. Cancer Sci 107:224–232
14. Jeong HS, Jones D, Liao S, Wattson DA, Cui CH, Duda DG, Willett CG, Jain RK, Padera TP (2015) Investigation of the lack of angiogenesis in the formation of lymph node metastases. J Natl Cancer Inst 107
15. Mikada M, Sukhbaatar A, Miura Y, Horie S, Sakamoto M, Mori S, Kodama T (2017) Evaluation of the enhanced permeability and retention effect in the early stages of lymph node metastasis. Cancer Sci 108:846–852
16. Freeman NE (1949) Lymphangiography in the diagnosis of chylangioma and lymphedema; a preliminary report. Am J Med 6:390–391
17. Kinmonth J, Taylor G, Harper RK (1955) Lymphangiography. Br Med J 1:940–942
18. Yamashita K, Shimizu K (2009) Evaluation of sentinel lymph node metastasis alone guided by three-dimensional computed tomographic lymphography in video-assisted breast surgery. Surg Endosc 23:633–640
19. Nakagawa M, Morimoto M, Takechi H, Tadokoro Y, Tangoku A (2016) Preoperative diagnosis of sentinel lymph node (SLN) metastasis using 3D CT lymphography (CTLG). Breast Cancer 23:519–524
20. Itkin M, Nadolski GJ (2018) Modern techniques of lymphangiography and interventions: current status and future development. Cardiovasc Intervent Radiol 41:366–376
21. Li L, Mori S, Sakamoto M, Takahashi S, Kodama T (2013) Mouse model of lymph node metastasis via afferent lymphatic vessels for development of imaging modalities. PLoS One 8:e55797
22. Shao L, Mori S, Yagishita Y, Okuno T, Hatakeyama Y, Sato T, Kodama T (2013) Lymphatic mapping of mice with systemic lymphoproliferative disorder: usefulness as an inter-lymph node metastasis model of cancer. J Immunol Methods 389:69–78
23. Tanaka Y, Komori H, Mori S, Soga Y, Tsubaki T, Terada M, Miyazaki T, Fujino T, Nakamura S, Kanno H, Sawasaki T, Endo Y, Nose M (2010) Evaluating the role of rheumatoid factors for the development of rheumatoid arthritis in a mouse model with a newly established ELISA system. Tohoku J Exp Med 220:199–206
24. Kochi T, Imai Y, Takeda A, Watanabe Y, Mori S, Tachi M, Kodama T (2013) Characterization of the arterial anatomy of the murine hindlimb: functional role in the design and understanding of ischemia models. PLoS One 8:e84047
25. Tada A, Horie S, Mori S, Kodama T (2017) Therapeutic effect of cisplatin given with a lymphatic drug delivery system on false-negative metastatic lymph nodes. Cancer Sci 108:2115–2121
26. Cabral H, Makino J, Matsumoto Y, Mi P, Wu H, Nomoto T, Toh K, Yamada N, Higuchi Y, Konishi S, Kano MR, Nishihara H, Miura Y, Nishiyama N, Kataoka K (2015) Systemic targeting of lymph node metastasis through the blood vascular system by using size-controlled Nanocarriers. ACS Nano 9:4957–4967
27. Fujii H, Horie S, Takeda K, Mori S, Kodama T (2018) Optimal range of injection rates for a lymphatic drug delivery system. J Biophotonics 11:e201700401
28. Dori Y, Zviman MM, Itkin M (2014) Dynamic contrast-enhanced MR lymphangiography: feasibility study in swine. Radiology 273:410–416
29. Harisinghani MG, Barentsz J, Hahn PF, Deserno WM, Tabatabaei S, van de Kaa CH, de la Rosette J, Weissleder R (2003) Noninvasive detection of clinically occult lymph-node metastases in prostate cancer. N Engl J Med 348:2491–2499
30. Fortuin AS, Bruggemann R, van der Linden J et al (2018) Ultra-small superparamagnetic iron oxides for metastatic lymph node detection: back on the block. Wiley Interdiscip Rev Nanomed Nanobiotechnol 10:e1471
31. Harrell MI, Iritani BM, Ruddell A (2007) Tumor-induced sentinel lymph node lymphangiogenesis and increased lymph flow precede melanoma metastasis. Am J Pathol 170:774–786
32. Alitalo A, Detmar M (2012) Interaction of tumor cells and lymphatic vessels in cancer progression. Oncogene 31:4499–4508